Supporting Information

Schwartz et al. 10.1073/pnas.0906382106

SI Text

Animals. Eight male Kyoto–Wistar rats and 8 male Wistar rats (Charles River Laboratory) were singly housed in transparent polycarbonate cages (20 × 25 × 22 cm) kept in light-tight isolation chambers, with ad libitum access to food and water at 20–25 °C. Unless otherwise noted, animals were maintained in LD 11:11 h; illumination (100–150 lux at cage level) was provided by white fluorescent tubes mounted in the top of the isolation chambers with no light in DD or during the dark phase of the LD cycle. Locomotor activity was continuously monitored by means of two crossed infrared photobeam detectors and collected using the Clocklab data collection program (Actimetrics). All experiments were performed in compliance with guidelines established by the University of Michigan University Committee on Use and Care of Animals, the University of Washington Animal Care and Use Committee and the National Institutes of Health Guide for the Care and Use of Laboratory Animals. All experiments were performed at the University of Michigan.

Surgery. Construction and implantation of transverse microdialysis probes was performed as described in ref. 1. Briefly, transverse probes consisted of two identical bases composed of blunt-tipped needles of two different diameters threaded into each other and bent into a hook with the needle tip perpendicular to the luers. One of the bases was connected to 2.5–3.5 cm of hollow microdialysis membrane (Spectrum Labs) and the other was set aside until surgery. A sharpened tungsten wire (ESPI Metals; Ashland, OR) was inserted into the open end of the microdialysis fiber and affixed with a small amount of epoxy. Before surgery, animals were deeply anesthetized, then placed in a stereotaxic instrument. A 2-cm transverse incision was made to expose the skull. Three surgical screws were placed in the top of the skull to anchor the microdialysis probe assembly, and one hole was made on each side of the skull, ≈2–3 mm below the top of the skull at the intraaural mark. The tungsten wire and fiber were threaded through the holes, and the wire was gently removed. The second probe base was connected to the microdialysis fiber and affixed with epoxy. The two bases were then anchored to the screws with dental cement. The incision was closed with sutures and animals were returned to their cages. To minimize disruption of the desynchronized motor activity, all surgeries occurred during the light phase of the LD cycle. Animals were allowed to recover for at least 24 h before melatonin sampling was initiated. All animals maintained a dual oscillatory pattern while in LD22, despite nonspecific increases in locomotor activity after dialysis probe implantation.

Microdialysis and HPLC Analysis. At the start of sampling, probes were connected to a peristaltic pump (Instech Laboratories) using PEEK tubing (Bioanalytical Systems) and a dual channel swivel (Instech) mounted above the cage to allow the animal to freely move. Animals were perfused with artificial cerebrospinal fluid (148 mM NaCl, 3 mM KCl, 1.4 mM $CaCl_2{\cdot}2H_2O$, 0.8 mM $MgCl_2{\cdot}6H_2O$, 0.8 mM $Na_2HPO_4{\cdot}7H_2O$, and 0.2 mM $NaH_2PO_4{\cdot}H_2O$) at a rate of 2 μL/min. For each animal three samples, each collected over 10 min, were taken per hour. Dialysates were separated in a reversed phase C18 high-performance liquid chromatography (HPLC) column (Supelco) at 30 °C. The mobile phase consisted of 22% (vol/vol) acetonitrile, 0.5 g/L heptane–sulfonic acid, 10 mM sodium acetate (pH 4.5), and 0.1 mM Na_2–EDTA. After separation, dialysates were quantified online using a fluorescence detector (Shimadzu). All sampling was computer controlled using the Shimadzu Class vp software. This technique allows high-resolution sampling of pineal melatonin profiles suitable for detailed circadian study (1–3). Of eight Wistar rats implanted with probes, three were removed from analysis due to probe failure.

Data Analysis. Desynchronized locomotor rhythms were verified via χ^2 periodogram analysis using El Temps (A. Díez-Noguera; Universidad de Barcelona, Barcelona). Percentages of variance in locomotor data were analyzed by a mixed repeated-measures ANOVA; percentages were arcsine transformed before analysis. For melatonin amplitude analyses (Fig. 4), daily melatonin peak concentrations for each individual were normalized by dividing by the average of all daily peak values for that individual to facilitate comparison between individuals. For all other analyses and plots, melatonin dialysate concentrations for each day were normalized to their 24-hour peak (13:00–13:00 EST) and are expressed as percentages of that daily peak for all phase analyses. For all animals, the circadian trends in the raw melatonin profiles were accurately reflected by the normalized data. Melatonin onsets and offsets were set at 20% of the daily peak (1). Melatonin onset and offset periods were calculated using eye-fitted regression lines in El Temps.

Forced Desynchronization Model

Model Equations. We simulated a set of two coupled oscillators forced by a Zeitgeber. The same set of equations is used for the general model of forced desynchronization using A and B oscillators (Fig. S2*A*), and a more specific model of LD cycle entrainment using the vl- and dmSCN as the coupled oscillators (Fig. 3*A*). The latter is structurally equivalent to the model proposed and analyzed by Kronauer (4) for the human circadian system controlling sleep–wake and temperature rhythms.

The two oscillators were simulated by coupled Pittendrigh–Pavlidis equations. In these equations, R and S are state variables, and a, b, c, and d are oscillator parameters. C_{AB} and C_{BA} are the coupling strengths of oscillator A on B and of oscillator B on A, respectively. Zeitgeber L is represented by square waves, which are zero except at intervals of duration L_{dur}, when they get fixed amplitude value L. These equations differ from the Pavlidis equation (5) by a parameter K, which is a small nonlinear term ($K = 1/[1 + 100R^2]$) formulated by W.T. Kyner (C. Pittendrigh and W. T. Kyner, personal communication). This parameter stabilizes the R variable by preventing it from approximating zero.

Oscillator A:

$$dR_A/dt = R_A - c_A S_A - b_A S_A^2 + (d_A - L) + K$$
$$dS_A/dt = R_A - a_A S_A + C_{BA} S_A$$

Oscillator B:

$$dR_B/dt = R_B - c_B S_B - b_B S_B^2 + (d_B - L) + K$$
$$dS_B/dt = R_B - a_B S_B + C_{AB} S_B$$

Simulations were performed using the CircadianDynamix software (www.neurodynamix.net), which is an extension of NeuroDynamix II (6). We used the Euler method for numerical integration, with 1,000 integration steps per 24-hour day. R was explicitly constrained from achieving negative values. Locomotor activity occurred every time the S variable in either the A or B oscillator (or the vl or dm oscillator) rose above some threshold

value, which we set to two-thirds of the maximum amplitude of this variable. Melatonin release occurred every time the S variable in the B oscillator (or the dm oscillator) rose above the same threshold value. A complete description of the simulation methods is described in refs. 7 and 8. The rationale behind the differential control of locomotor activity and melatonin release by the two oscillators is that whereas periodogram analysis of the locomotor activity output clearly shows two components (a 22-h light-associated component and a ≈24-h dissociated component) the melatonin rhythm does not show these dual oscillatory components but rather a relative-coordinated ≈24-h rhythm. This is in part because during the light phase locomotor activity can be expressed but melatonin is never released. Furthermore, in contrast to increased locomotor activity, melatonin is only released during the dark phase when the dissociated dm oscillator is in the appropriate phase, indicating that the entrained vlSCN cannot sustain the release of melatonin on its own.

Simulation of Forced Desynchronization. For a configuration in which a Zeitgeber of fixed amplitude acts on two mutually coupled oscillators (A and B) with extremely weak coupling, A and B might express relatively independent dynamics (7), with minor influences on each other. We consider the situation where $T < \tau_A < \tau_B$, for a set of four T values, such that $T_4 < T_3 < T_2 < T_1$ and T_1 is within the ranges of entrainment of both oscillators; T_2 is within the range of entrainment of A and just outside of B; T_3 is just outside the range of entrainment of A and B; and T_4 is far outside the ranges of entrainment of both oscillators.

Fig. S2 shows simulations of weakly coupled A and B oscillators forced by a Zeitgeber with period T equal to T_1, T_2, T_3 and T_4. Under T_2 and T_3, entrainment of A and B are dissociated by the Zeitgeber and forced desynchronization occurs. In this state, oscillator B is neither entrained nor free-running; rather, it is in relative coordination (9). Locomotor activity controlled by an oscillator in relative coordination is typically characterized by a "zigzagging" actogram pattern. Under T_4, the period of the coupled system (25 h) is longer than under true free-running conditions (24.4 h); the same trend was shown in previous experimental data with forced desynchronized rats (10, 11). Thus, the Zeitgeber acts systematically on the coupled oscillators even when it fails to entrain one or both of them. Simulations of this particular configuration of oscillator properties and couplings also show an experimentally observed decrease of period of the non-entrained component as T is increased (10, 12).

Output of an Oscillator under Relative Coordination. In Fig. S4, relative coordination of a single oscillator subjected to periodic pulses is shown as predicted by a hypothetical phase response curve (PRC) using the same schematics presented by Moore-Ede et al. (13). For simplification, light-induced phase shifts and oscillator amplitude recoveries are assumed to be instantaneous. The control of locomotor activity (or melatonin release if light inhibition is accounted for) is also assumed to be instantaneous, so that activity phase reflects oscillator phase accurately. These assumptions are adopted to highlight the origin of the large phase shifts and the resulting relative coordination.

Consider a single oscillator A with intrinsic period τ_A subjected to a Zeitgeber with period T. As predicted by the discrete entrainment model (14–16), entrainment is attained when there exists a Φ_A value in the PRC corresponding to a phase shift $\Delta\Phi$ that exactly matches the difference in the periods:

$$\Delta\Phi(\Phi_A) = T - \tau.$$

The Zeitgeber pulses necessarily fall, after transient cycles, on this phase Φ_A and then fall each cycle on this phase, entraining the oscillator. In Fig. S4*A*, Φ_A lies in the advance region because Zeitgeber period T is shorter than τ and entrainment results, therefore, by daily phase advances.

Relative coordination, however, occurs by an alternation of quasi-free-running activity and transient, near-entrainment states (Fig. S4*B*, *C*). It is important to note that the limits of entrainment of an oscillator to a Zeitgeber with fixed amplitude correspond to the upper and lower values of the PRC. Oscillator A has an intrinsic $\tau > T$. This explains why melatonin onsets occur later each day at some phases of the relative coordination as observed in Wistar rats (Fig. 2; see *Strain Differences* below), contributing to shortening of bout duration observed under forced desynchronization. τ_A is such that there is no phase Φ_A in the advance region that can generate a phase shift $\Delta\Phi$ sufficiently large to match the difference between τ and T. There is a limited time when pulses fall sequentially in the advance region of the PRC resulting in a transient, near-entrainment to T (pulse number 8 −13 in Fig. S4*B*). Because there is no phase Φ_A in the advance region that can generate a phase shift $\Delta\Phi$ (Φ_A) = $T - \tau$, pulses will eventually depart from the advance and fall on the delay region of the PRC (shown by pulses 14, 15 in Fig. S4*B*), which sum up with the $\tau > T$ to generate a very long delay. Then pulses fall on the dead zone of the PRC where $\Delta\Phi = 0$ (pulses 16,17 in Fig. S4*B*) and the oscillator's phase is not influenced. The oscillator is "free-running" in this region only. After pulse 10 the sequence repeats itself, generating a periodic zigzag pattern with an overall period corresponding approximately to τ plus the summation of phase shifts (advances and delays) achieved through the advance-delay cycles. This additive effect can be seen when the same simulations are performed in an oscillator with $\tau = 26$ h (Fig. S4*C*), resulting in relative coordination similar to data published in refs. 4 and 17. The difference is because the oscillator's longer intrinsic period sums with the periodic phase delays, contributing to an increase in the inclination of the relative coordination pattern. Thus, when a system of coupled oscillators is under forced desynchronization and the non-entrained oscillator is in relative coordination, its observed period under the desynchronizing T cycle does not represent its intrinsic τ value, because it is not truly free-running. Of note, the large periodic phase delays shown in Fig. S4 may actually represent an underestimation of the real delays observed experimentally, because in this simulation the PRC is kept constant throughout relative coordination. Oscillator amplitude is expected to periodically change under this condition (Fig. 4*A*), and consequently the PRC should also change. By this logic, PRC amplitude is expected to be maximal when the oscillator amplitude is minimal (18), corresponding to the day of delay shift, when the system is in misaligned phase.

When ($T - \tau$) is far outside the maximum $\Delta\Phi$ value of the PRC, non-entrainment occurs. The Zeitgeber hits the oscillator at various phases that span the whole circadian cycle without ever phase-locking the oscillator. Once again, the oscillator is not truly free-running in this condition because it is periodically phase shifted by the Zeitgeber.

Strain Differences. Fig. S5 shows simulations of a set of two systems differing only in the coupling strength that the dm oscillator exerts over the vl oscillator. The main differences between the Kyoto and Wistar strains are faithfully simulated by these two systems. The system with greater coupling strength exerted by the dm oscillator does not completely dissociate and shows a shorter overall period as the Kyoto rats do, even though the individual τ of the vl and dm oscillators was not changed in our simulation. These results are also consistent with the finding that the percentage of variance explained by the $\tau > 24$ bout in the periodogram analysis was larger in Kyoto than in Wistar rats.

Predictions of the Model. Several testable predictions emerge from our model. (*i*) Entrainment to a 22-h T cycle with a shorter than

11-h light phase should result in demasking of the melatonin offset and reveal the full relative coordination profile of the dmSCN. (*ii*) The amplitude of rhythmic clock gene expression within the dmSCN when its phase is misaligned with the vlSCN′s phase should be initially low upon release into constant conditions and increase with successive cycles. We are currently testing this prediction using *ex vivo* slices of the *Per1-luciferase* rat (19). (*iii*) Exposure to LD cycles longer than 24-h should result in relative coordination of the vlSCN, because our model proposes that its inherent period is shorter than 24 h, and a complex pattern of melatonin release. In contrast, if the vlSCN is passively driven by light, longer period LD cycles should result in an entrained rhythm of melatonin release with this period. (*iv*) If the vlSCN is passively driven by light, its phase-specific response to light, characterized by an increase in the expression of *cFos* and *Per1* only during the subjective night, should depend on the phase of the dmSCN and its input to the vlSCN. In other words, the vlSCN should not show increased gene expression when the pulse is presented during the dmSCN subjective day in forced desynchronized rats. In contrast, if the vlSCN is a true circadian oscillator, its response to light may be intrinsically gated and be at most modulated by the dmSCN circadian phase.

1. Borjigin J, Liu T (2008) Application of long-term microdialysis in circadian rhythm research. *Pharmacol Biochem Behav* 90:148–155.
2. Liu TC, Borjigin J (2005) Free-running rhythms of pineal circadian output. *J Biol Rhythms* 20:430–440.
3. Liu TC, Borjigin J (2005) Reentrainment of the circadian pacemaker through three distinct stages. *J Biol Rhythms* 20:441–450.
4. Kronauer RE, Czeisler CA, Pilato SF, Moore-Ede MC, Weitzman ED (1982) Mathematical model of the human circadian system with two interacting oscillators. *Am J Physiol* 242:R3–17.
5. Pavlidis T (1973) *Biological Oscillators: Their Mathematical Analysis* (Academic, New York).
6. Friesen WO, Friesen JA (2010) *NeuroDynamix II* (Oxford Univ Press, Oxford), in press.
7. Oda GA, Menaker M, Friesen WO (2000) Modeling the dual pacemaker system of the tau mutant hamster. *J Biol Rhythms* 15:246–264.
8. Oda GA, Friesen WO (2002) A model for ''splitting'' of running-wheel activity in hamsters. *J Biol Rhythms* 17:76–88.
9. von Holst E (1939) Die relative koordination als phenomen und als methode zentralvervöser funktionsanalyse. *Ergebn Physiol* 42:228–306.
10. Campuzano A, Vilaplana J, Cambras T, Diez-Noguera A (1998) Dissociation of the rat motor activity rhythm under T cycles shorter than 24 hours. *Physiol Behav* 63:171–176.
11. de la Iglesia HO, Cambras T, Schwartz WJ, Diez-Noguera A (2004) Forced desynchronization of dual circadian oscillators within the rat suprachiasmatic nucleus. *Curr Biol* 14:796–800.
12. Cambras T, Chiesa J, Araujo J, Diez-Noguera A (2004) Effects of photoperiod on rat motor activity rhythm at the lower limit of entrainment. *J Biol Rhythms* 19:216–225.
13. Moore-Ede MC, Sulzman FM, Fuller CA (1982) *The Clocks that Time Us. Physiology of the Circadian Timing System* (Harvard Univ Press, Cambridge).
14. Pittendrigh CS, Daan S (1976) Functional-analysis of circadian pacemakers in nocturnal rodents. 5. Pacemaker structure—clock for all seasons. *J Comp Physiol* 106:333–355.
15. Daan S, Pittendrigh CS (1976) Functional-analysis of circadian pacemakers in nocturnal rodents. 2. Variability of phase response curves. *J Comp Physiol* 106:253–266.
16. Johnson CH, Elliott JA, Foster R (2003) Entrainment of circadian programs. *Chronobiol Int* 20:741–774.
17. Richter CP (1977) Heavy water as a tool for study of the forces that control length of period of the 24-hour clock of the hamster. *Proc Natl Acad Sci USA* 74:1295–1299.
18. Winfree AT (1980) *The Geometry of Biological Time* (Springer, New York).
19. Yamazaki S, et al. (2000) Resetting central and peripheral circadian oscillators in transgenic rats. *Science* 288:682–685.

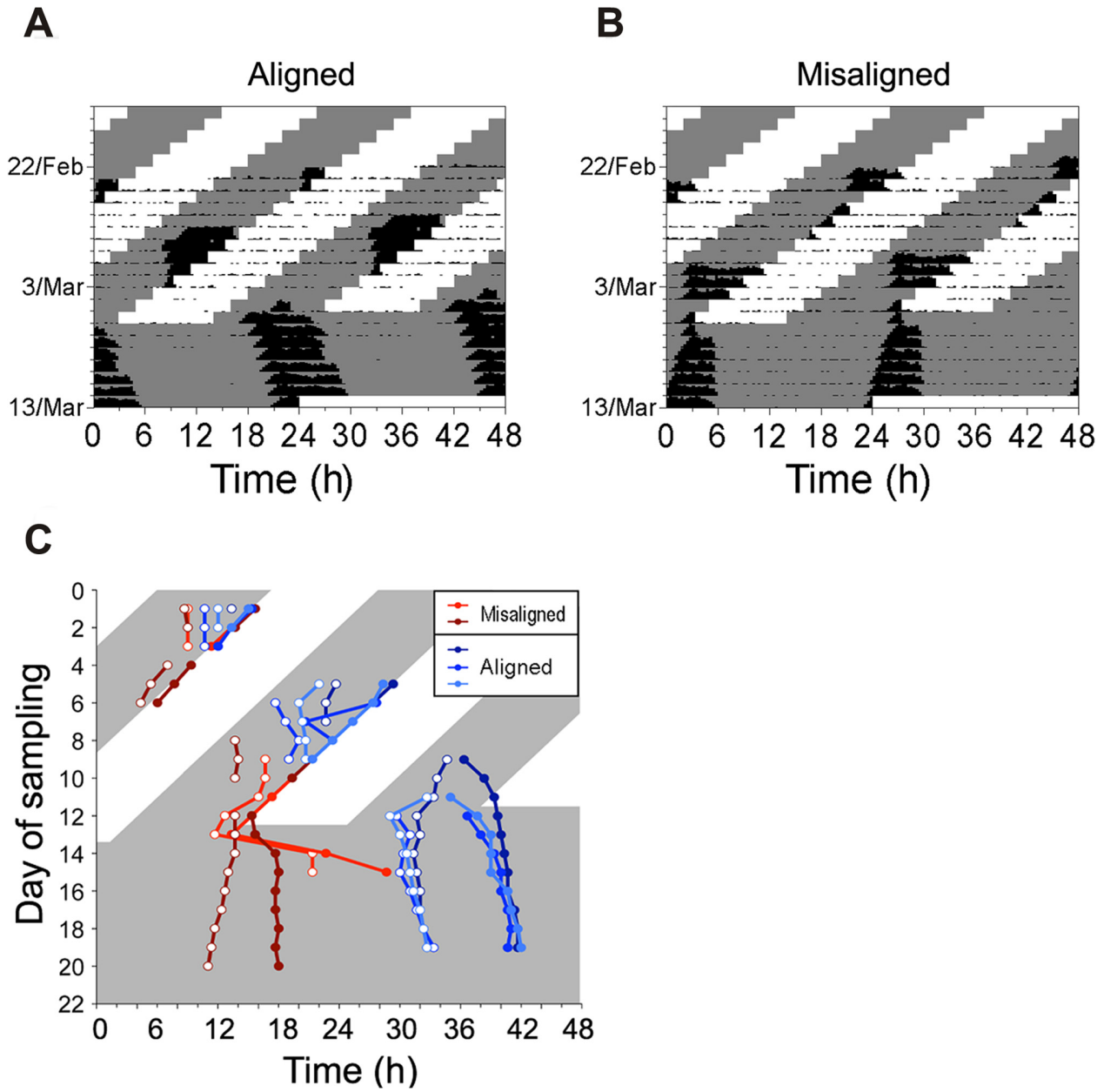

Fig. S1. The profile of melatonin release upon release from LD22 desynchrony into constant darkness. (*A* and *B*) Representative actograms depicting melatonin profiles after release into DD from aligned (*A*) or misaligned (*B*) phases. (*C*) combined melatonin onsets (open circles) and offsets (colored circles) for all individuals; each color represents a single animal. Data presented in *C* is repeated in Fig. 2*A*.

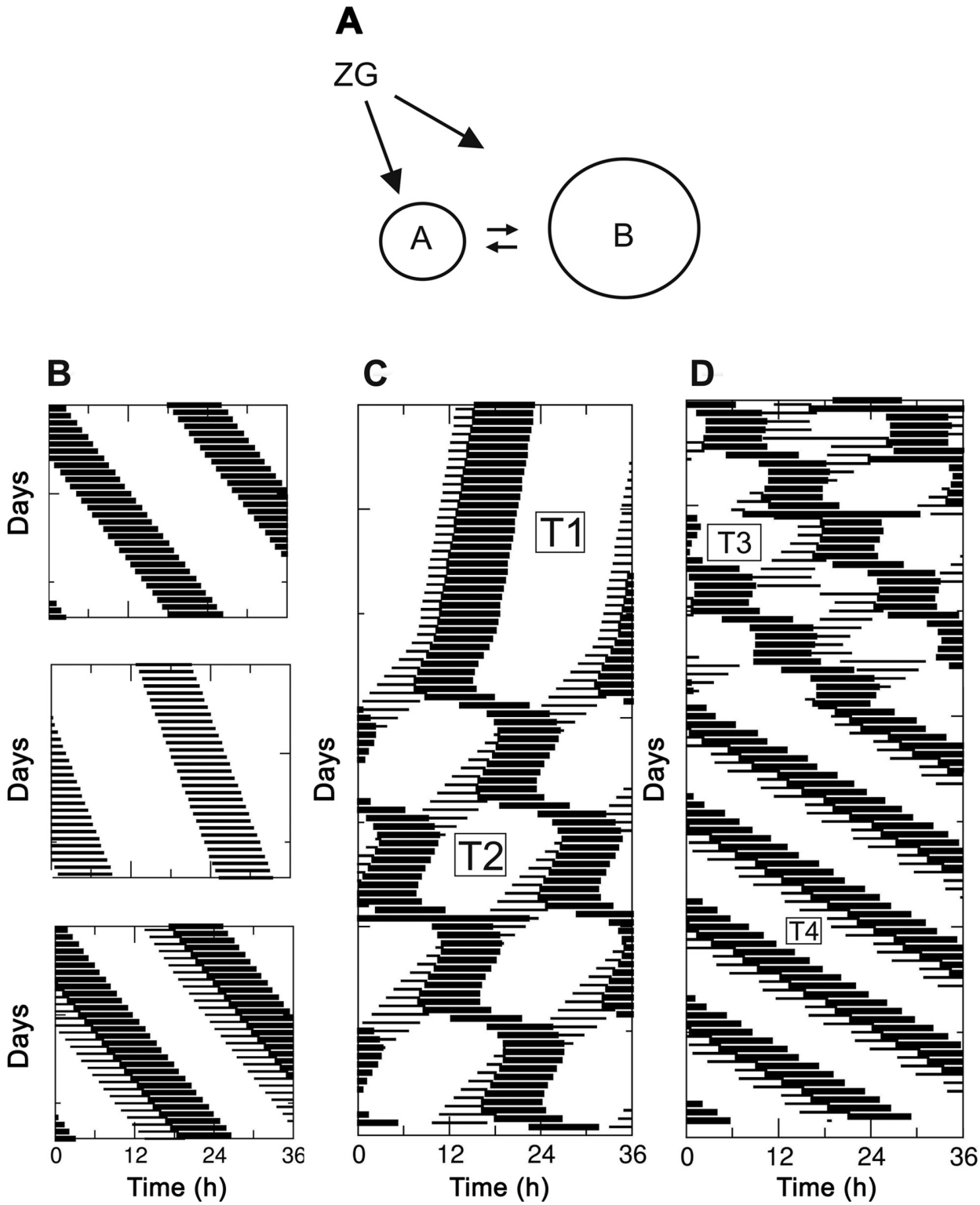

Fig. S2. Simulations of activity rhythms controlled by coupled oscillators forced by *T* cycles. (*A*) Schematic diagram of coupled oscillators forced by a Zeitgeber. Small arrows indicate the influence that the dynamics of one oscillator exerts on the other. Relative size of the circles indicates relative period (τ) values for the oscillators. (*B*) (*Top*) Free-running B oscillator, $\tau_B = 24.43$ h. (*Middle*) Free-running A oscillator, $\tau_A = 24.25$ h. (*Bottom*) Free-running coupled A and B oscillator, $\tau_{AB} = 24.4$ h. (*C*) Coupled A and B oscillators under *T* cycles $T_1 = 23.9$ h (*Upper*) and T2 = 23.4 h (*Lower*). (*D*) Coupled A and B oscillators under *T* cycles $T_3 = 22.8$ h (*Upper*) and T4 = 15 h (*Lower*), period of non-entrained oscillators $\approx$ 25 h. Pittendrigh–Pavlidis oscillator equation parameters for C–E: $a_A = 0.85$; $b_A = 0.3$; $c_A = 0.8$; $d_A = 0.5$; $a_B = 0.85$; $b_B = 0.3$; $c_B = 0.5$; $d_B = 0.5$. Coupling parameters: $C_{AB} = C_{BA} = 0.01$. Zeitgeber: $L_{dur} = 1$; $L = 1$.

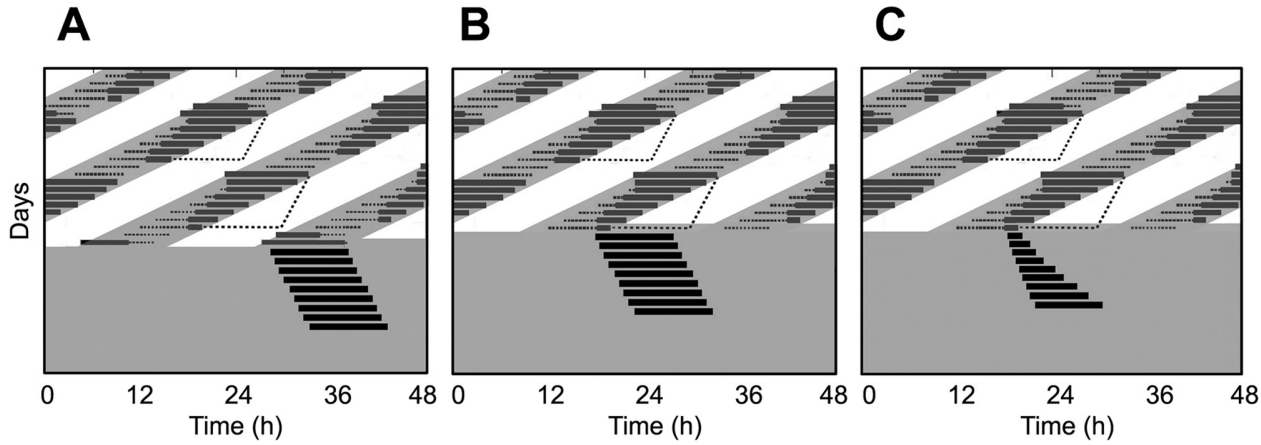

Fig. S3. Schematic patterns of melatonin secretion upon release of a forced desynchronized system into DD. Projection of melatonin profiles if release into DD starts after: a matching day in which the melatonin peak was wide (*A*); a conflict day in which the melatonin peak was narrow and in the case this narrowing is only explained by masking by the LD cycle (*B*) or in the case this narrowing is explained also by a reduction of the amplitude of the dm oscillator (*C*). Gray bars during 22-h LD cycle represent melatonin bouts generated by simulation of coupled oscillators under forced desynchrony. Black bars after release into DD represent hypothetical projections of melatonin bouts. The three projections schematized upon release into DD are not generated by computer simulations because the Pittendrigh–Pavlidis equations display fast recovery dynamics when Zeitgebers are removed and are not therefore appropriate for simulating slow, aftereffects of entrainment. Our hypothetical predictions are based on the established knowledge that circadian oscillators of rodents do display aftereffects in response to previous entrainment conditions (14).

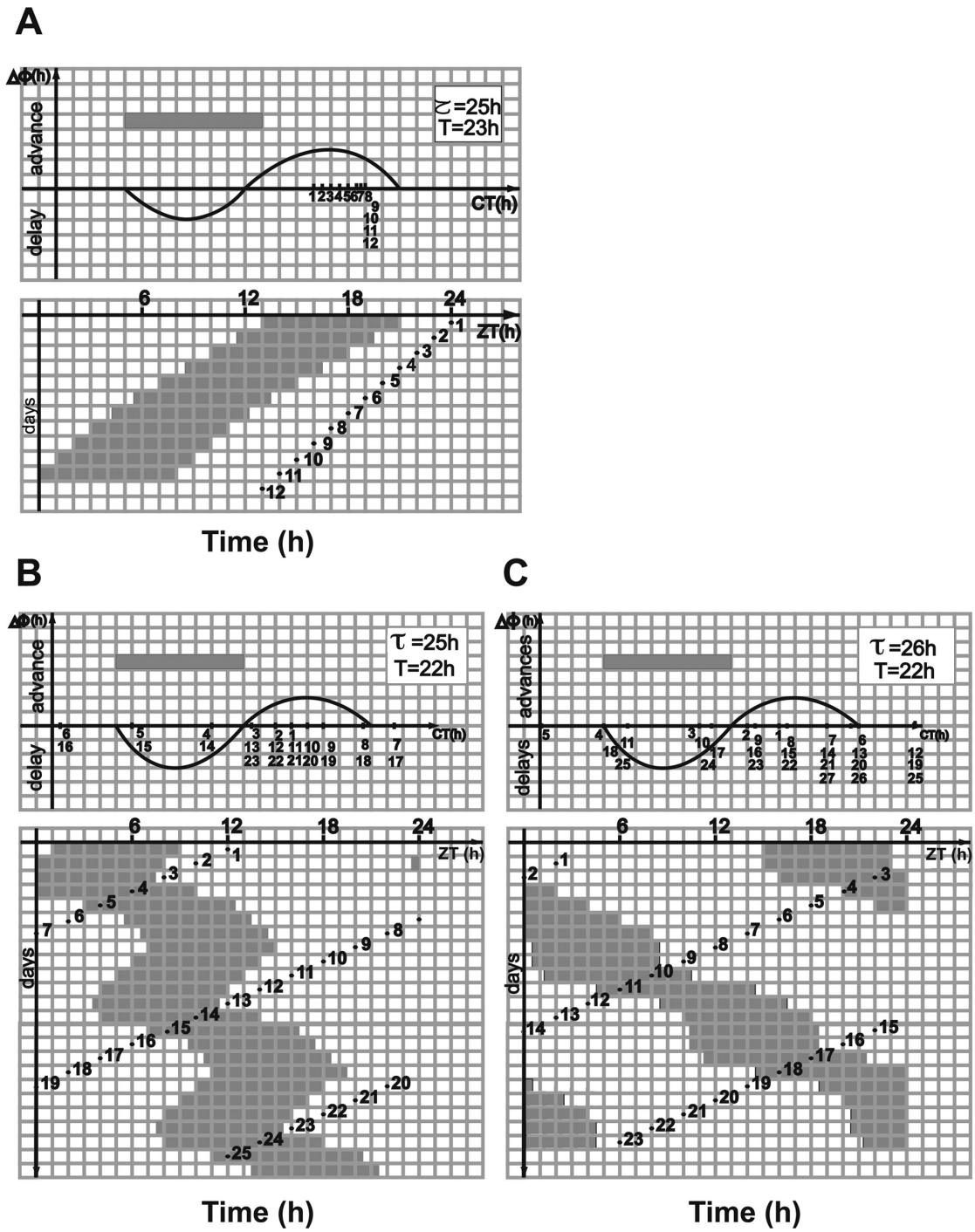

Fig. S4. Dynamics of an oscillator subjected to *T* cycles, as predicted by PRCs. (*A*) Entrainment to a *T* cycle. (*Upper*) schematic PRC of oscillator with $\tau = 25$ h. Numbers indicate phases hit by the periodic pulses. Pulses 1 to 7 evoke transient phase shifts. Entrainment is attained after pulse 8. For simulation, 1 circadian time (CT) hour $\approx$ 1 Zeitgeber time (ZT) hour. (*Lower*) Simulated actogram of activity controlled by the oscillator. Numbers indicate pulse phases, which are presented with $T = 23$ h. In the example above, the first pulse hits oscillator at $\Phi = (3$ h after activity end), which corresponds to a $\Delta\Phi = -2.5$ h. The next activity bout starts after $(\tau+\Delta\Phi = 25 - 2.5 = 22.5)$ h in ZT. (*B*) Relative coordination to a *T* cycle. (*Upper*) schematic PRC of the oscillator with $\tau = 25$ h. Periodic pulses are presented with $T = 22$ h, *a* value which is outside the range of entrainment according to its PRC. (*Lower*) Simulated actogram of activity controlled by the oscillator. (*C*) Relative coordination of an oscillator with longer τ to the same *T* cycle ($T = 22$ h). (*Upper*) Schematic PRC of the oscillator with $\tau = 26$ h. PRC shape is approximated by the same of the $\tau = 25$ oscillator, for easier comparison. (*Lower*) Simulated actogram of activity controlled by the oscillator. The relative sizes of delay and advance regions of the PRCs in *A*–*C* are different to make the entrainment or relative coordination patterns more obvious. As a consequence of these changes, the cross-over point between delays and advances also changes to maintain a smooth PRC.

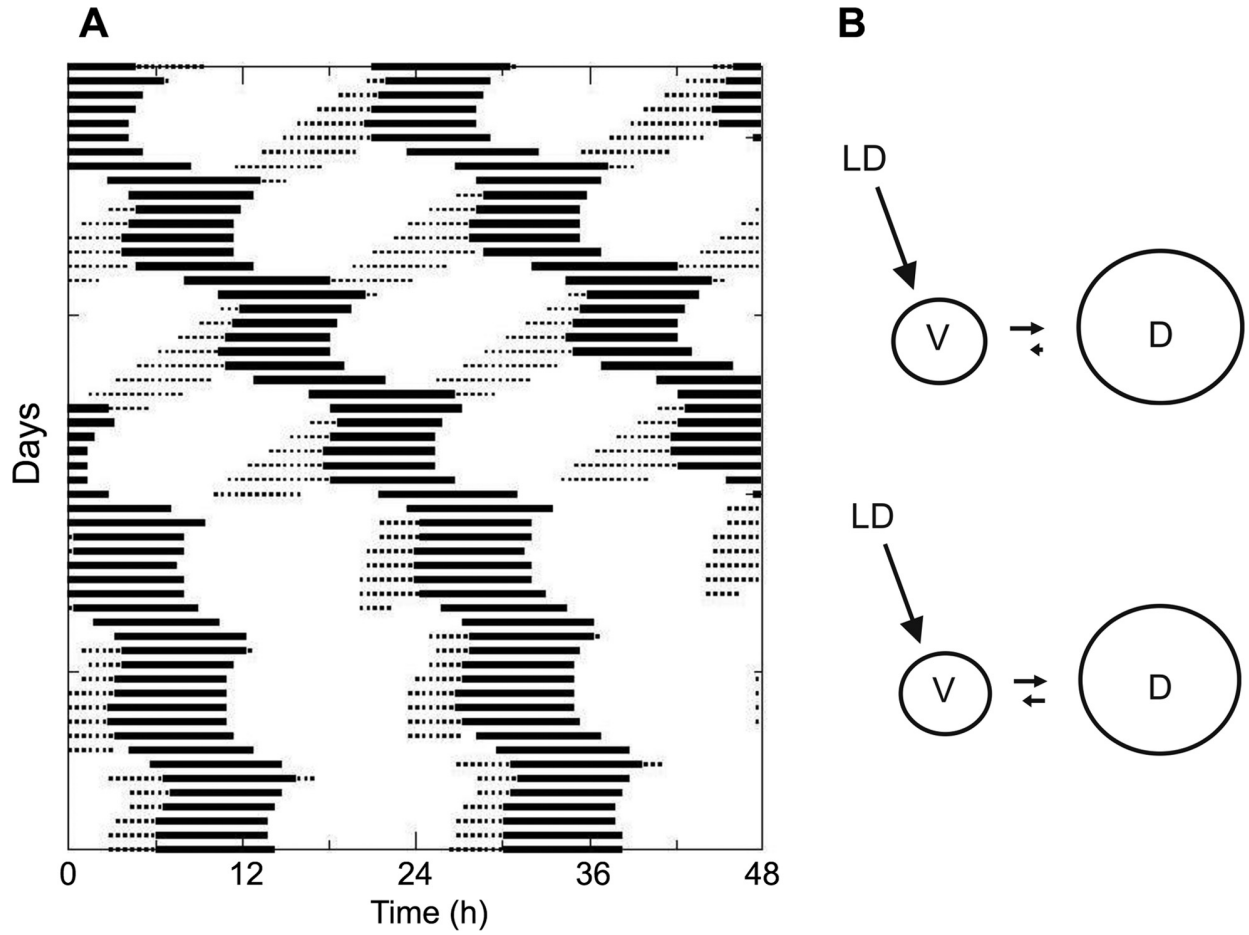

Fig. S5. Changes of coupling strength between oscillators faithfully represent rat strain differences in dissociation. Simulation of two coupled vl (thin line) and dm (heavy line) oscillators (*A*) shown schematically in the *Right* (*B*). (*Upper*) Weak coupling strength from dm to vl results in dissociation between vl and dm. $C_{VD} = 0.14$; $C_{DV} = 0.05$. (*Lower*) Stronger coupling influence from dm to vl prevents dissociation. $C_{VD} = 0.14$; $C_{DV} = 0.12$. Parameters: Oscillator vl with $\tau_V = 23$ h, ($a_V = 0.85$; $b_V = 0.3$; $c_V = 1.1$; $d_V = 0.5$); oscillator dm with $\tau_D = 24.3$ h, ($a_D = 0.85$; $b_D = 0.3$; $c_D = 0.75$; $d_D = 0.5$); LD duration = 1; LD amplitude = 1; LD period = 22 h.